Na6Li4MO4(CO3)4 (M = W and Mo): An Alternative Electrolyte for High-Temperature Electrochemical Cells

Cyrille Galven, Valérie Albin, Simon Hubert, Virginie Lair, Armelle Ringuede, Marie-Pierre Crosnier-Lopez, Françoise Le Berre

$Na_6Li_4MO_4(CO_3)_4$ (M = W, Mo) : an alternative electrolyte for high temperature electrochemical cell

Cyrille Galven,[a] Valérie Albin,[b] Simon Hubert,[b] Virginie Lair,[b] Armelle Ringuede,[b] Marie-Pierre Crosnier-Lopez,[a] Françoise Le Berre [a,]*

a : Institut des Molécules et Matériaux du Mans (IMMM), UMR CNRS 6283, Le Mans Université, Avenue Olivier Messiaen, 72085 Le Mans Cedex 9, France

b : Chimie ParisTech, PSL University, CNRS, Institut de Recherche de Chimie Paris, 75005 Paris, France

TOC

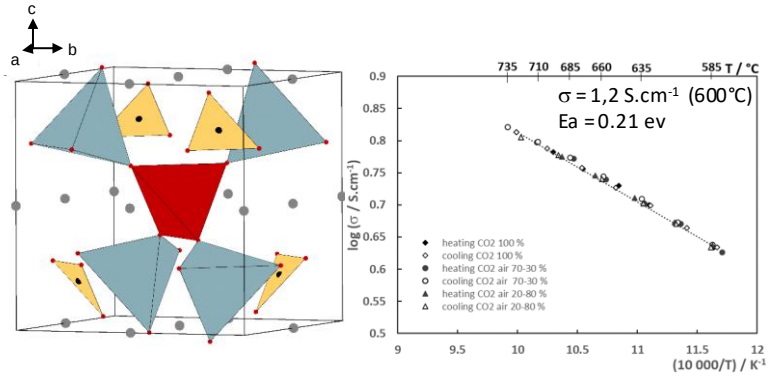

Synopsis

This paper deals with the synthesis and the characterization of two new acentric oxycarbonates $Na_6Li_4MO_4(CO_3)_4$ (M = W, Mo). The structure solved by X-ray diffraction is described in the P-43m space group ($a \approx 7.15$ Å). Electrical measurements performed on solid pellets and molten salt bath show that the conductivity is purely ionic. Both oxycarbonates present a stable electrical behavior with Ea close to 1.5 eV in the solid state and 0.21 eV above 600°C.

Abstract

Two new acentric oxycarbonates $Na_6Li_4MO_4(CO_3)_4$ (M = W, Mo) were synthesized via a conventional solid-state route. Their structure was determined from X-ray diffraction data on single crystal. $Na_6Li_4MO_4(CO_3)_4$ (M = W, Mo) crystallizes in the acentric cubic P-43m space group (a ≈ 7.15 Å). It is composed of MLi_4O_{16} units built from MO_4 and LiO_4 tetrahedra and linked by CO_3^{2-} groups to form a 3D framework in which Na^+ ions are inserted. We showed from DSC and powder X-ray diffraction experiments that the melting is congruent (T ~ 525°C). In the solid and molten forms, conductivity was measured for both oxycarbonates by electrochemical impedance spectroscopy with three various gas compositions (CO_2 100 vol%, CO_2-air 70-30 vol%, CO_2-air 20-80 vol%). Each time, the stability of the electrical behaviour was checked via heating and cooling cycles. The conductivity of both solid and molten phases is purely ionic and in the same order of magnitude as for the classical molten alkali electrolyte made of Li-Na or Li-K carbonates. As activation energies are also comparable, those new oxycarbonates appear to be promising electrolytes for electrochemical devices.

Keywords

New oxycarbonate, MCFC, ionic conductivity, acentric structure, electrolyte

I. Introduction

In the current energy context, the reduction of greenhouse gases is a major concern. Among the ways considered to reduce environmental impact, hydrogen appears to be an unavoidable decarbonized vector. Its conversion will be the most interesting if it feeds a fuel cell. Among the fuel cell technologies developed, the molten carbonate fuel cell (MCFC) has already reached a certain maturity. The system has an electrical efficiency of around 50%, and the overall efficiency can be even higher, reaching 80%. These cells are used on an industrial scale, with projects in South Korea and the United States, for example. The industrial leader in MCFCs, Fuel Cell Energy, has now more than 50 installations worldwide following the start of commercialization of MCFC in 2003. The largest unit, 59 MW, is in Hwaseong, South Korea. More recently, molten carbonate cells have attracted much attention for CO_2 capture and separation.[1, 2, 3]

Fuel cell is an electrochemical system that converts chemical energy into electricity, via an electrochemical reaction. It is composed of two electrodes, an anode and a cathode, where oxidation and reduction reactions occur respectively, and an electrolyte (ionic conductor) that separates them. In MCFC, the electrolyte is a molten mixture of alkali metal carbonates – usually a binary mixture at eutectic composition of lithium and potassium carbonates, or lithium and sodium carbonates. It is retained in a porous ceramic matrix, made of $LiAlO_2$, electrically insulating. As the matrix is non-conductive, ionic conductivity is ensured by Li^+, Na^+ or K^+ cations and carbonate anions through the molten carbonate phase. As references, it is worth mentioning the high level of molten carbonate eutectics conductivities,.e.g. 1.14 $S.cm^{-1}$ and 1.82 $S.cm^{-1}$ at 600°C respectively for the mixture Li_2CO_3-K_2CO_3 62:38 mol% and Li_2CO_3-Na_2CO_3 52:48 mol%[4]. Nevertheless, electrolyte management is one of the key points of the MCFC technology as it leads to degradation of performances.[5, 6, 7] For instance, the high corrosivity of carbonates limits the electrochemical devices lifespan because of Ni-based

cathode dissolution or metallic bipolar plates corrosion. Moreover, electrolyte composition is modified during operation because of Li consumption due to *in situ* lithiation of NiO electrode (at short-term) and further evaporation, especially for potassium-based electrolytes. Then research on electrolytic membrane management is of great interest. Different options are considered such as the improvement of the matrix in terms of mechanical resistance but also ionic conductivity, the refuelling of the electrolyte with chosen additives, the modification of the alkali carbonates electrolyte itself.[8, 9, 10] Herein, we explore the modification of the electrolyte by adding, not alkaline or alkaline-earth elements, but transition metals, which are very common, less expensive. Molybdenum and tungsten oxides are frequently used in the industry as gas sensor, catalyst, electrochromics, lubricants…[11, 12] Then, some of their physicochemical properties such as thermal and chemical stability, catalytic properties, corrosion resistance, etc., seem relevant to electrochemical application. Moreover, Lacorre et al. discovered fast oxygen ion-conducting electrolytes based on $La_2Mo_2O_9$ (LAMOX). This electrolyte for Solid Oxide Fuel Cell (SOFC) presented interesting ionic conductivity (8.02×10^{-2} S cm^{-1} at 800 °C).[13, 14] More recently, LAMOX based electrolytes ($La_{1.8}Dy_{0.2}Mo_{2-x}W_xO_9$) containing both Mo and W elements were synthesized. The electrical conductivity and the activation energy of these electrolytes under air atmosphere, at 800 °C were measured and the substitution of Mo by W led to an increase in conductivity.[15]

We present here two new ionic conductors oxycarbonates, $Na_6Li_4MO_4(CO_3)_4$ (M = W, Mo). After structural and physicochemical characterization, their ionic conductivity was measured by electrochemical impedance spectroscopy in the solid and molten forms under different gas atmospheres, at different temperatures in order to qualify their potential interest as electrolyte for high temperature electrochemical devices.

II. Experimental section

II.1. Synthesis

The two oxycarbonates $Na_6Li_4MO_4(CO_3)_4$ (M= W, Mo) were prepared under powder form by solid state synthesis, starting from stoechiometric mixtures of dehydrated Na_2CO_3 (Acros Organics, 99.8 %), Li_2CO_3 (Alfa Aesar, > 99 %) and MoO_3 (Alfa Aesar, 99.95 %) or WO_3 (Alfa Aesar, 99.8 %). The resulting mixtures (~ 1g) were pressed into pellets, placed in an alumina boat and heated at 495°C for 36 hrs with two intermediate grindings to obtain the desired well crystallized oxycarbonates.

The structure was solved from single crystal data for $Na_6Li_4WO_4(CO_3)_4$. For this, single crystals were synthetized from melted mixture of stoichiometric composition heated 6 hrs at 550°C and slowly cooled (0.03°C.min^{-1}).

The large quantity of sample required for conductivity measurements in the molten state (~ 160g) led us to find another synthesis route to reduce the time of preparation. For this purpose, we used the melt casting way with the same precursors. After a mixing step of the starting compounds weighted in stoichiometric ratio, the mixtures (M = Mo and W) were introduced in a nickel crucible and heated to 575 °C for 45 minutes before being casted on a nickel foil. After grinding and in order to homogenize, the powder was then heated at 495°C for 24 hrs.

II.2. Analytical Measurements

II.2.1. Infrared (IR) Spectroscopy. For IR spectroscopy, a Bomen Michelson MB120 FTIR spectrometer with a diamond-anvil cell as a microsampling device was used. The spectral resolution was 4 cm^{-1} in the 650−4000 cm^{-1} range.

II.2.2. Scanning Electron Microscopy (SEM)

The chemical analyses were performed on a JEOL JSM 6510LV microscope equipped with the EDS OXFORD system and using the AZtec software.

II.2.3. X-ray Diffraction. The purity and the crystallinity of the powder samples were checked from Powder X-ray Diffraction (PXRD) patterns recorded in air with a PANalytical Empyrean diffractometer using Cu Kα radiation.

The refinements were performed with Fullprof software[16] using a pseudo-Voigt function to describe the peak shape. The background level was determined manually before being refined. Thermal PXRD patterns were collected with the same diffractometer completed with a high temperature attachment XRK900. They were recorded under static air between 30 and 430°C every 50°C with the following experimental conditions: 10–120° 2θ, with a step of 0.013° and a counting time of 150 seconds per step.

The single crystal diffraction data were acquired on a Bruker APEX II Quazar (4-circle Kappa goniometer) single crystal diffractometer equipped with a micro-source (IμS microfocus source - Mo Kα) and a CCD 4 K detector. Included in the software package WINGX, the program SHELXL-2014/7 was used to solve and refine the crystal structure.[17]

II.2.4. Second-Harmonic Generation (SHG) Measurement. A SHG test is commonly used to prove the crystal noncentrosymmetry.[18] If a significant second harmonic light is generated when the sample is irradiated by a short light pulse, then the SHG test is positive, and one can be sure that the crystal structure is non centrosymmetric. The test was performed on polycrystalline $Na_6Li_4MO_4(CO_3)_4$ (M= W, Mo) samples using a microchip Q-switched Nd:YAG laser from Teem Photonics, which emits at the wavelength of 1064 nm short optical pulses of 0.6 ns (full width at half-maximum) and 10 μJ, at the repetition rate of 5 kHz. The pump laser beam was focused by a microscope objective ×6.3 onto the powder sample introduced in a Lindemann capillary tube with 0.7 mm internal diameter. This microscope objective was also used to collect the backscattered SHG light at 532 nm.

II.2.5. Thermal Analysis

Differential Scanning Calorimetry was carried out using a SETARAM SETSYS EVOLUTION in order to precisely determine the thermal behavior of $Na_6Li_4MO_4(CO_3)_4$ (M= W, Mo). The sample (from 30 to 50 mg in a 90 µL alumina crucible) has been heated and cooled under different air/CO_2 mixtures with a flow rate of 20 mL/min (CO_2 100 vol%; CO_2-air 70-30 vol%; and CO_2-air 20-80 vol%) between 40°C and 800°C at a rate of 2°C min^{-1}.

II.3. Electrochemical measurements

Conductivity measurements were carried out by electrochemical impedance spectroscopy (EIS) using a Solartron Analytical Energylab potentiostat. Signal frequencies were scanned from 1MHz to 0.1 Hz, with 10 points per decade. The measurements were performed separately for both solid and molten phases, as a function of temperature, under atmospheric pressure. The temperature range for all the experiments was 250-470°C for the solid phase and 600-750°C for the molten phase referring to DSC analysis. All the electrochemical measurement were performed from the same powder batch.

II.3.1 Conductivity in the solid phase (250-470°C): Pellets of $Na_6Li_4MO_4(CO_3)_4$ (M= W, Mo) oxycarbonates were prepared from 0.5g of powder, first uniaxially pressed at 1000 bars (100 MPa) using a 10 mm die. The pellets were then isostatically pressed at 4500 bars (450 MPa) for 1mn and sintered at 495°C for 2h. Electrodes were deposited as thin gold films by RF sputtering technique on both parallel sides of the pellets. Then electrical behaviour was characterized through EIS using this 2-electrodes symmetric configuration in single atmosphere set-up. The chosen amplitude for EIS analysis is 100 mV, in respect to the system linearity. To ensure repeatability, measurements were repeated at least 3 times. A total flow rate of 65 mL.min^{-1} was used with 3 various gas compositions: CO_2 100 vol%, CO_2-air 70-30 vol%, and CO_2-air 20-80 vol%.

II.3.2 Conductivity in the molten phase (600-750°C): the electrochemical cell, an alumina cylindrical crucible placed in an alumina reactor, was described elsewhere.[19] The electrolyte consists of 75 g of the previous synthetized oxycarbonate, $Na_6Li_4MO_4(CO_3)_4$ (M = W, Mo). Oxycarbonate powders are dried before use and kept in a drying oven at 130°C. The system, at atmospheric pressure, is left at least 12 h, under atmosphere of interest before analysis to ensure its equilibrium. Two gold planar electrodes set in parallel, were used. Each plate has a surface of 1 cm^2 (1x1 cm^2) and is 0.5 mm thick (Au plate, 99.99%, AMTS, France). The distance between both electrodes is kept constant and equal to 2 cm. The gold plates were previously polished on SiC grinding paper (P1200, P2400, P4000) and then rinsed under ultrasonics in water-ethanol 50-50 vol% before each experiment. The signal amplitude used for EIS analysis is 5 mV, respecting the system linearity. A total flow rate of 50 $mL.min^{-1}$, was used with 3 various gas compositions: CO_2 100 vol%, CO_2-air 70-30 vol%, and CO_2-air 20-80 vol%.

III. Results and discussion

In the aim to modify the chemical formulation of the classical electrolyte Li_2CO_3:Na_2CO_3 used in molten carbonate cells, we decided to add transition metals. We obtained for some compositions, PXRD patterns that corresponded to mixtures of known phases with in addition, a same set of intense lines. As these lines did not match to any pattern listed in the databases, we performed preliminary characterizations to determine the exact composition of this new phase and synthesize it as a single phase sample.

III.1. IR Spectroscopy

An IR spectrum (Figure 1) was recorded as described in the experimental part. This spectrum reveals three bands (1450, 1083 and 873 cm^{-1}) characteristic of the presence of the CO_3^{2-} carbonate group: the broad and intense band at 1450 cm^{-1} is attributed to the antisymmetric υ_3

vibration mode, while the two others, narrower bands at 1083 and 873 cm^{-1} are respectively attributed to the symmetric vibration mode υ_1 and the bending mode υ_2. [20]

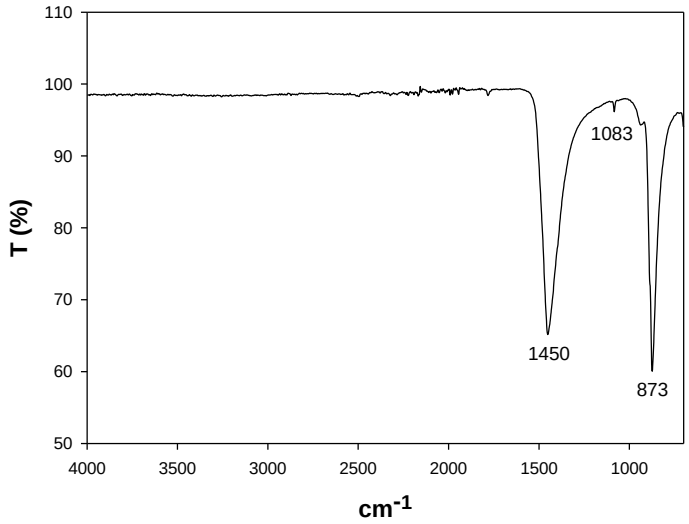

Figure 1: IR spectrum of $Na_6Li_4WO_4(CO_3)_4$

III.2. Scanning Electron Microscopy

The chemical analysis performed on the powder sample confirmed the simultaneous presence of sodium, tungsten (or molybdenum), oxygen and carbon with molar ratios Na/W ≈ 5.2 and Na/C ≈ 1.3. As Li can't be evidenced by EDS, we also performed a synthesis without lithium. The resulting PXRD pattern does not show the set of intense Bragg reflections previously observed but corresponds to a mixture of known phases (Figure S1) implying thus the necessary presence of lithium in the target material.

III.3. Structure determination

III.3.1. Powder X-ray diffraction

After many attempts, we succeeded to obtain one pure sample with the following ratio: Na/Mo = 6 and Na/Li = 1.5. For this composition, all the diffraction reflections of the PXRD pattern could be indexed in a cubic cell with a parameter of 7.1508 Å (Figure 2).

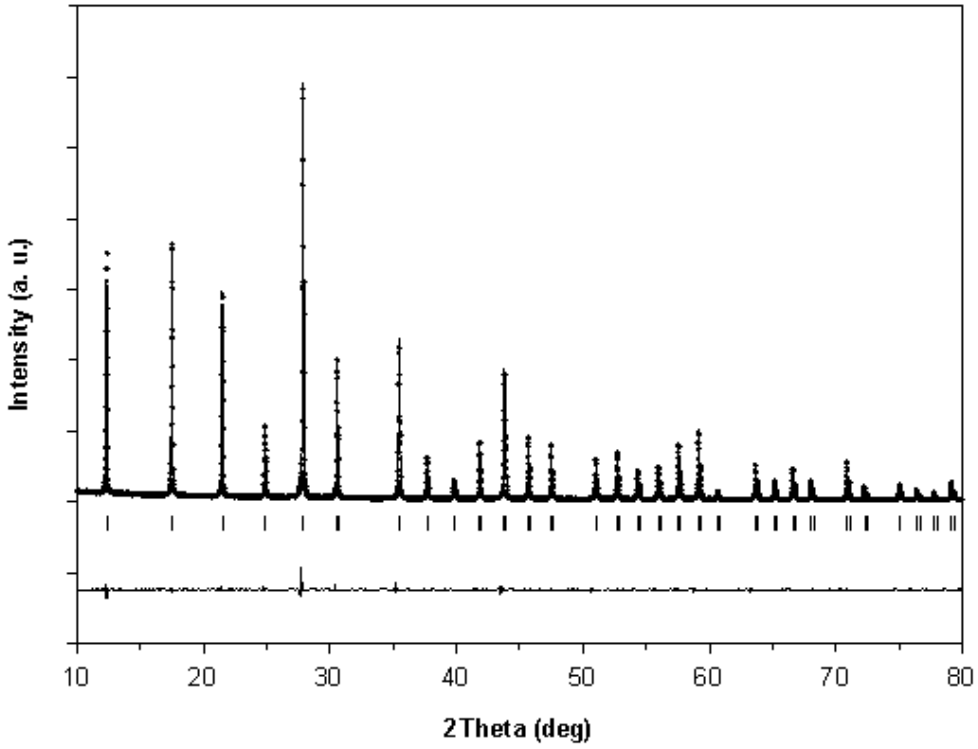

Figure 2 : Observed, calculated and difference PXRD patterns of $Na_6Li_4MoO_4(CO_3)_4$ in the Pm-3m space group by full pattern matching refinement mode. The verticals bars are related to the calculated Bragg reflection positions

No extinction condition was observed leading necessarily to the extinction symbol P--- compatible with five space groups: two centric groups (Pm-3 (no. 200) and Pm-3m (no.221)) and three acentric groups (P23 (no. 195), P432 (no.207), P-43m (no.215)). The two Pm-3 and Pm-3m space groups have been excluded because the SHG test showed a positive answer (Figure 3) implying then a non-centrosymmetric space group.

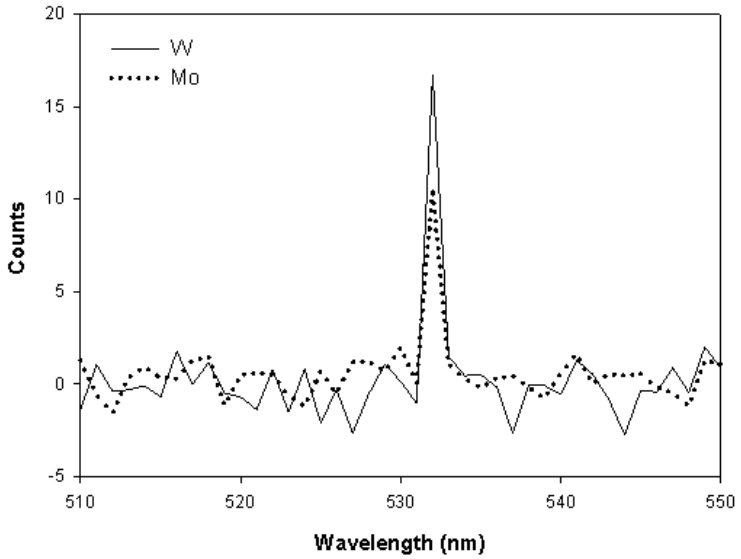

Figure 3: SHG signal for $Na_6Li_4WO_4(CO_3)_4$ and $Na_6Li_4MoO_4(CO_3)_4$

In the case of M = W, a similar cubic cell (7.153 Å) explained all the intense Bragg reflections of the pattern. However, additional weak reflections were systematically observed corresponding to Na_2WO_4 (ICDD Card No. 01-070-1040) (Figure S2).

III.3.2. Single crystal diffraction

The presence of light atoms as lithium and oxygen in the formulation led us to perform the structural determination from a single crystal (M = W). It was obtained as described in the experimental section and carefully selected for the X-ray diffraction data collection. The data analysis suggested the m-3m Laue class compatible with only two of the previous three acentric space groups: P432 (no.207) or P-43m (no.215). A starting model was quickly obtained in the P-43m space group with six atomic positions: 1b, 3c, 3d, 12i and two 4e positions. Given the relative scattering power of tungsten atom compared to that of the others,

it was unambiguously located at 1b site while the other sites were assigned to Na (3c and 3d), C (4e) and O (4e and 12i) taking into account the usual anion-cation distances. Fourier difference syntheses allowed to complete the structure with one site (4e) in a tetrahedral

environment which can then be associated to lithium cations according to Li-O distances. The resulting chemical formula is then $Na_6Li_4WO_4(CO_3)_4$. With absorption correction, anisotropic displacement parameters and a weighting scheme, the final refinement converged to good reliability factors R = 0.0181 for the 348 data with $I > 2\sigma(I)$ and for all the data with a final difference synthesis featureless. The sample and crystal data for $Na_6Li_4WO_4(CO_3)_4$ are given in Table 1 while Table 2 gathers information on the data collection and on the structure refinement.

Table 1: Sample and crystal data for $Na_6Li_4WO_4(CO_3)_4$

Symmetry	Cubic
Space group	P -4 3 m (no. 215)
Cell parameter a /Å	7.1529(3)
Volume /Å^3	365.97(5)
Z	1
Formula weight /gmol^{-1}	633.59
$Density_{calc}$	2.966
Temperature /K	296(2)
Wavelength /Å	Mo Kα, 0.71073
Crystal size /mm	0.132 ×0.210 × 0.389
Absorption coefficient /mm^{-1}	8.162

Table 3 gives the atomic coordinates, the equivalent isotropic atomic displacement parameters and the bond valence sums while selected atomic distances and anisotropic atomic displacement parameters are given respectively in Tables 4 and S1.

Table 2: Data collection and structure refinement for $Na_6Li_4W(CO_3)_4O_4$

Range registered :	
2θ max /°	69.62
h; k; l min, max	-10, 7; -6, 11; -4, 11
Reflections collected	2456
Independent reflections	348 [R(int) = 0.0398]
Absorption correction	Multi-scan
Max. and min. transmission	0.4120 and 0.1430
Refinement method	Full-matrix least-squares on F^2
Refinement program	SHELXL-2014/7 (Sheldrick, 2014)
Function minimized	Σ w $(F_o^2-F_c^2)^2$
Data / restraints / parameters	348 / 0 / 22
Goodness-of-fit on F^2	1.140
Weighting scheme	$w = 1/[\sigma^2(F_o^2)+(0.0272P)^2]$ where $P = (F_o^2+2F_c^2)^2/3$
Extinction coefficient	0.106(9)
Final Fourier difference :	
Largest diff. peak and hole /Å^3	0.574 and -1.028
R.M.S. deviation from mean /eÅ^{-3}	0.125
Final R indices	348 data; I>2σ(I) R1 = 0.0181, wR2 = 0.0407
	all data R1 = 0.0181, wR2 = 0.0407

Table 3: Atomic coordinates, equivalent isotropic atomic displacement parameters (Å^2) and bond valence sums (Σ**)** for $Na_6Li_4W(CO_3)_4O_4$ (S.G.: P -4 3 m)

	Site	s.o.f.	x	y	z	U_{eq}	Σ	(Σ_{exp})
W	*1b*	1	0.5	0.5	0.5	0.0095(2)	6.3	(6)
Na1	*3d*	1	0.5	0.0	0.0	0.0192(5)	1.0	(1)
Na2	*3c*	1	0.0	0.5	0.5	0.0220(6)	1.0	(1)
Li	*4e*	1	0.209(2)	0.209(2)	0.209(2)	0.012(4)	1.2	(1)
C	*4e*	1	0.808(1)	0.808(1)	0.808(1)	0.013(2)	4.0	(4)
O1	*12i*	1	0.2664(3)	0.2664(3)	0.9538(5)	0.0193(6)	2.1	(2)
O2	*4e*	1	0.3587(7)	0.3587(7)	0.3587(7)	0.039(2)	2.0	(2)

(U_{eq} is defined as one third of the trace of the orthogonalized U_{ij} tensor)

Table 4: Selected interatomic distances (Å) for $Na_6Li_4W(CO_3)_4O_4$

(mean distances are given in italic)

W tetrahedra	Na polyhedron	Li tetrahedra	C polyhedra
W-O2 : 4×1.751(8)	**Na1-O1 :** 8×2.5559(5)	**Li-O2 :** 1×1.86(2)	**C-O1 :** 1.286(3)
<W-O> = 1.751 Å	**Na2-O1 :** 4×2.386(3)	**Li-O1 :** 3×1.916(8)	*<C-O> = 1.286 Å*
	Na2-O2 : 4×2.9370(9)	*<Li-O> = 1.90 Å*	
	<Na-O> = 2.609 Å		

The refined crystal structure of $Na_6Li_4WO_4(CO_3)_4$ is displayed in Figure 4.

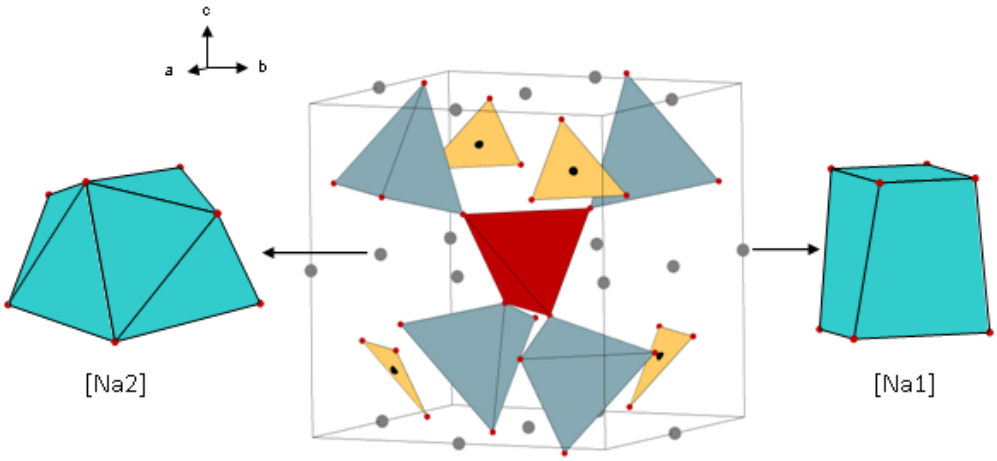

Figure 4: View of the $Na_6Li_4WO_4(CO_3)_4$ structure showing an isolated WLi_4O_{16} unit, CO_3^{2-} groups and the NaO_8 polyhedra (distorted cube for Na1 and trigonal dodecahedron for Na2)

In this structure, the tungsten and the lithium atoms are both in a tetrahedral environment. The tungsten is surrounded by four O2 to form a perfect WO_4 tetrahedron while the lithium is surrounded by one O2 and three O1. Each O2 corner is shared with one LiO_4 tetrahedron, building thus WLi_4O_{16} units isolated from each other and which can be noted $WO2_4Li_4O1_{12}$

(Figure 4). The "free" O1 corners of the WLi_4O_{16} units participate in the formation of CO_3^{2-} carbonate group so that each CO_3^{2-} group links three WLi_4O_{16} units together (Figure 5).

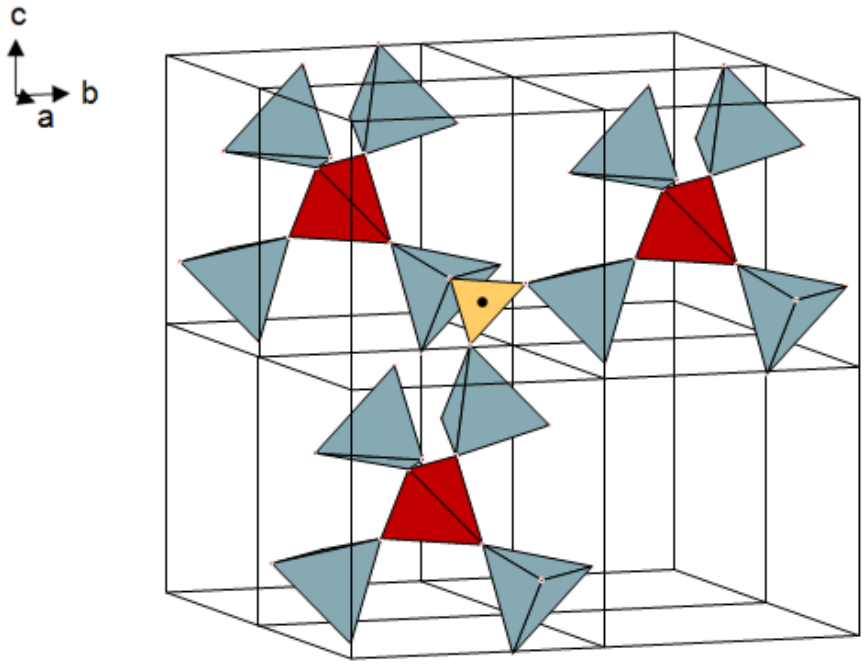

Figure 5: Partial view of $Na_6Li_4WO_4(CO_3)_4$ structure showing how a CO_3^{2-} group connects three WLi_4O_{16} units together

Such arrangement creates large cavities (coordination number 8) which accommodate the sodium ions: Na1 is located in a distorted cube while Na2 is in a trigonal dodecahedron (Figure 4).

From a distance point of view, the Table 4 shows that the mean distance for all cations are in good agreement with the Shannon table[21] (1.77, 2.53, 1.94 and 1.27 Å respectively for W, Na, Li and C taking into account their coordination number) leading consequently to bond valence sums close to the expected values (Table 3).

At this stage, it is interesting to ask whether this structure could have been described in the P432 space group (no.207) although the structure obtained in P-43m (no.215) seems quite relevant. A quick comparison of the positions of these two groups shows that the location of

the tungsten and sodium atoms can be transposed easily directly from one group to the other: 1b for W and 3d, 3c for Na in both groups. For lithium and carbon, both are located on two 4e sites (x, x, x) in P-43m group with a x value for carbon (0.808) very close to the -x lithium value (0.209). These two positions could then correspond to one 8g position of the P432 group, meaning then that the four lithium atoms and the four carbon atoms would be statistically distributed over the eight equivalent positions of the 8g site while they are located on their own site in the P-43m space group. Concerning the two anionic positions, the 12i site (x, x, z with z ~ 0.95) in the P-43m group could correspond to the 12i (0, y, y) site in the P432 group with z value set to zero while the 4e site for its part can be transposed to the 8g site with the same x value but a half occupancy rate. Then, since it's possible to transpose all the structure from the P-43m to the P432 space group, we performed a complete structure refinement in this new space group. We observed first that, with absorption correction, anisotropic displacement parameters and a weighting scheme, the final refinement converged to much higher reliability factors R = 0.0622 compared to 0.0181 in the P-43m space group. Secondly, the equivalent isotropic atomic displacement parameters for Li and C (8g site) factor is about 50 times higher than the two values observed for these cations in the P-43m space group. Moreover, a split of this 8g position is suggested by the SHELXL program.[17] This implies that the Li/C ordering highlighted in the P-43m space group can't be correctly transposed in P432 meaning that the P-43m space group should be chosen to describe the $Na_6Li_4WO_4(CO_3)_4$ structure.

For $Na_6Li_4Mo(CO_3)_4O_4$, the structure was successfully refined from PXRD data by directly applying the refined model for tungsten which is consistent with the similarity of the two PXRD patterns. The refining results for $Na_6Li_4Mo(CO_3)_4O_4$ are given in Figure S3 and Table S2.

III.4. Thermal analysis

According to DSC analysis a very sharp endothermic peak has been observed for both oxycarbonates (Figures 6 and S4, respectively T2 and T4), characterizing the melting of the solid powder.

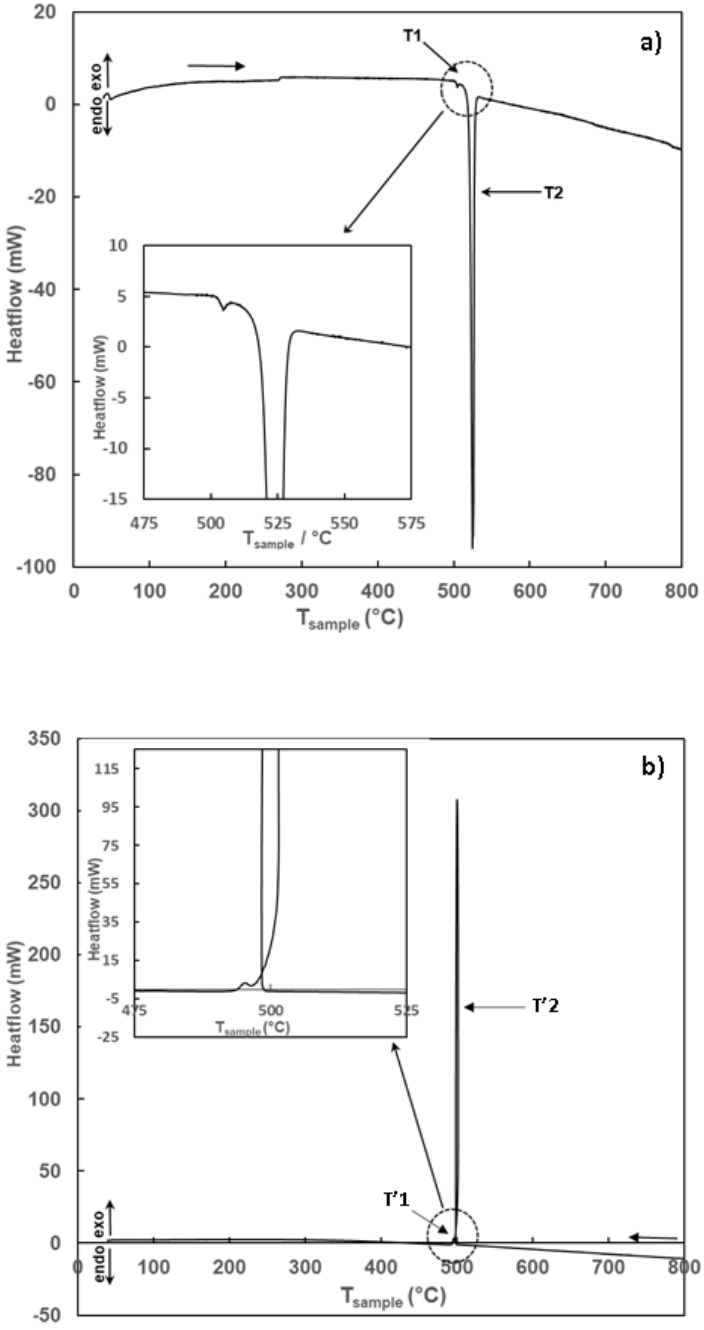

Figure 6: DSC curves of $Na_6Li_4MoO_4(CO_3)_4$ oxycarbonate, (a) heating at 2°C.min^{-1} in 100% CO_2 and (b) cooling at 2°C.min^{-1} in 100% CO_2

The melting point of the molybdenum phase ($Na_6Li_4MoO_4(CO_3)_4$) is 521°C whereas the melting point of the tungsten phase ($Na_6Li_4WO_4(CO_3)_4$), is 528 °C. Those two melting points are quite close to the melting point of the classical eutectic carbonates, Li_2CO_2-Na_2CO_3 52:48 mol% which is 501°C.[22] The PXRD patterns of the samples recorded before and after heating being identical (figure S5), we could conclude that the melting of our oxycarbonates is congruent, explaining then the route used to prepare the samples (see experimental section). It is worth noting that a very small and thin peak (T_1, Figure 6) is observed in the molybdenum phase, at 503°C, and in the tungsten phase (512°C, T3, Figure S4), indicating that the powder may contain a small excess of Li-Na carbonates, from the synthesis. This value, higher than for eutectic composition may be explained by the presence of remaining lithium and sodium carbonate at a different composition, especially when many syntheses are carried out in order to obtain a huge amount of oxycarbonates. DSC analysis registered during the cooling step showed also two peaks corresponding to the recrystallisation of the two phases described before, with the same relative intensities as during heating. For both oxycarbonates, these two peaks are obviously slightly lower than the melting peaks.

Nevertheless, in order to highlight possible subtle structural changes, PXRD patterns were collected up to 430°C so as not to reach their melting temperature. For both oxycarbonates, no particular transformation was evidenced (Figure S6) except a classical left shift of the Bragg reflections, reflecting a progressive increase of the cell parameter with temperature. Using the P-43m space group, the PRXD patterns refinement was quite satisfactory in this temperature range and a linear evolution of the cell parameter was observed (Figure S7 and Table S3) leading to the expansion coefficient $\alpha_a = 2.1\ 10^{-5}$ and $2.6\ 10^{-5}$ °C^{-1} for Mo and W oxycarbonates respectively.

III.5. Electrochemical measurements

Conductivity measurements have been carried out using Electrochemical Impedance Spectroscopy (EIS) for both molten oxycarbonates (in the temperature range 600°C to 750°C) and pellets of oxycarbonates (in the range 250-470°C). As molten carbonate phases required CO_2 to ensure the chemical equilibrium and avoid decarbonation of the system, different gaseous composition at atmospheric pressure were chosen. For each gas composition (20, 70 or 100 vol% of CO_2), the impedance of the two oxycarbonates was measured at different temperatures, during one heating and cooling cycle. The material conductivity was calculated from the electrolyte resistance (intercept at high frequencies of the diagram and the real part Z') as illustrated in Figure S8 and Figure S9 for both, solid pellet and molten salt.

III.5.1. Oxycarbonates pellets (250°C ≤ T ≤ 470°C)

The conductivity variation of a $Na_6Li_4MoO_4(CO_3)_4$ pellet varies linearly as a function of the reverse temperature whatever the CO_2 content in the gas phase (Figure 7). Thus it follows a single Arrhenius law in all the temperature range explored for these solid pellets.

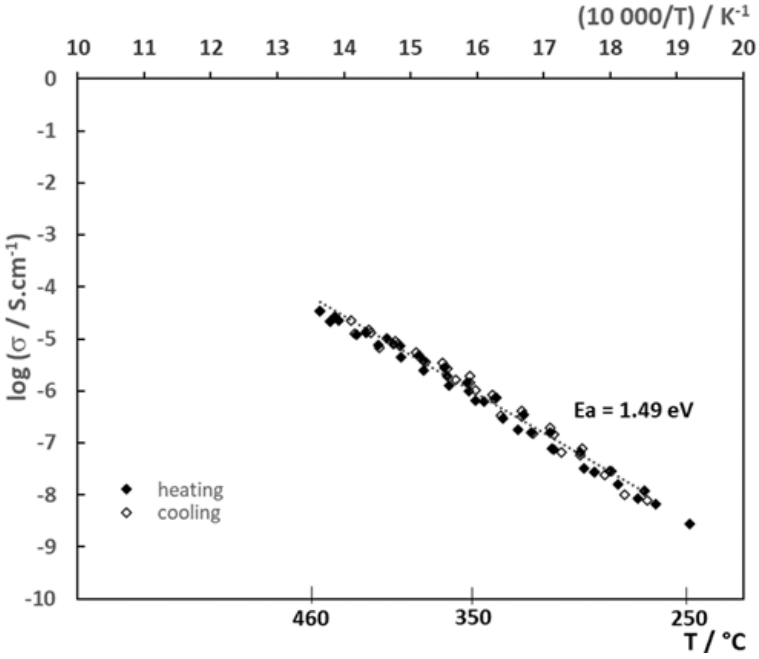

Figure 7: Arrhenius diagram of $Na_6Li_4MoO_4(CO_3)_4$ solid phase for three atmosphere compositions (CO_2 100%, CO_2:air 70:30, CO_2:air 20:80) and during one heating/cooling cycle each time.

Moreover, both heating and cooling cycle are overlayed without any hysteresis phenomenon and no influence of the CO_2 content is observed (Figure 7). The activation energy calculated from the slope is 1.49 eV of this figure. This behavior is comparable for $Na_6Li_4WO_4(CO_3)_4$ (Figure S10) and the activation energy is then a little bit slower, Ea = 1.45 eV. So, for both oxycarbonates, a stable electrical behavior is observed during a heating/cooling cycle whatever the CO_2 content (from 20 to 100 vol%). The conductivity is therefore independent of the atmosphere, which is consistent for an electrolyte material, showing pure ionic conductivity in these two compounds. Its value of 10^{-4} S.cm^{-1} at 480°C is nevertheless 10 times lower than YSZ (the state of art Solid Oxide Fuel Cell electrolyte) and 100 times lower than Gd-doped ceria, considered as a potential electrolyte in lower operating temperature range than with YSZ.[23] Furthermore, the activation energy determined for solid oxycarbonate compositions is highly higher compared to the ones associated to GDC or YSZ, 0.8 eV and 1 eV respectively. It is worth mentioning that the oxycarbonates were sintered at 495°C, much lower than the 1350°C required for GDC or YSZ, and the final density is *de facto* lower. Thus the conductivity of the oxycarbonate pellets is strongly affected by some porosity which cannot be avoided. It must be reminded that at higher temperature the two oxycarbonate phases are molten, thus cannot be densified.

III.5.2. Molten oxycarbonates (600°C ≤ T ≤ 750°C)

Above the melting point, (T>600°C), the conductivity variation of $Na_6Li_4MO_4(CO_3)_4$ (M = W, Mo) follows also a single Arrhenius law in the whole temperature range whatever the CO_2 gas content (Figures 8 and S11).

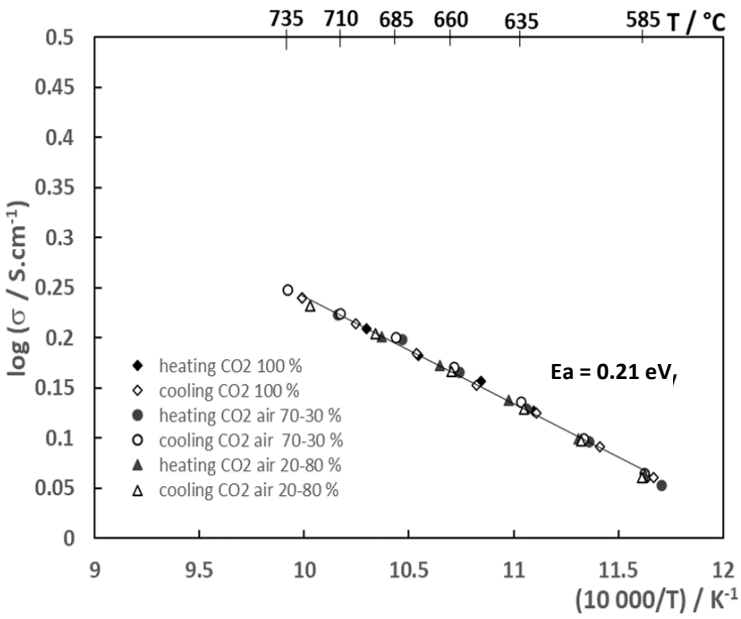

Figure 8: Arrhenius diagram of the molten $Na_6Li_4MoO_4(CO_3)_4$ phase as a function of the atmosphere composition (CO_2 100%, CO_2:air 70:30, CO_2:air 20:80) and during one heating/cooling cycle each time.

It is important to mention that the same electrical behavior is observed during heating and cooling steps, as discussed for solid phases. That means that no decarbonation of the oxycarbonate phases occurs in the conditions used for the measurements, probably thanks to CO_2 presence in the surrounding atmosphere. For both $Na_6Li_4MoO_4(CO_3)_4$ and $Na_6Li_4WO_4(CO_3)_4$, the ionic conductivity, 1.24 $S.cm^{-1}$ and 1.06 $S.cm^{-1}$ respectively for Mo- and W-based oxycarbonates are comparable to the usual molten carbonate eutectic mixtures: slightly lower than $(Li,Na)_2CO_3$ conductivity, i.e. 1.82 $S.cm^{-1}$ at 600°C but slightly higher than $(Li,K)_2CO_3$, i.e. 1.14 $S.cm^{-1}$ at 600°C. The equivalent activation energy of 0.21 eV is typical of cations and anions transport mechanisms in these media. This value is consistent with classical molten carbonate eutectics,[4, 19] meaning that these two new compounds could find potential applications such as electrolyte in high temperature fuel cell.

IV. Conclusion

The two new oxycarbonates, $Na_6Li_4MO_4(CO_3)_4$ (M = W, Mo) presented in this paper have been characterized by complementary techniques: IR spectroscopy, SHG test, EDS and thermal analysis, X-ray diffraction. Their structure, solved from a single crystal of $Na_6Li_4WO_4(CO_3)_4$, is described in the acentric P-43m space group with a = 7.1529(3)Å as cell parameter. It is composed of MLi_4O_{16} units built from a MO_4 tetrahedron sharing each of its corners with one LiO_4 tetrahedron. Three MLi_4O_{16} units are linked together by a CO_3^{2-} group forming thus a 3D framework in which Na ions are inserted. From DSC and PXRD, we showed that the melting of the two oxycarbonates is congruent and around T ≈ 525°C. Electrical measurements were performed on solid pellets (T < 500°C) and molten salt bath (T > 600°C) in different atmospheres containing however CO_2 to avoid decarbonation of the mixture. At low temperature (T < 500°C), both oxycarbonates present a stable electrical behavior during heating and cooling cycles, with an activation energy close to 1.5 eV. At high temperature (T > 600°C), when the oxycarbonates are melted, the activation energy is stable at 0.21 eV. It is worth noting that from conductivity value, the oxycarbonates containing W appears to be a little bit less performing than the one containing Mo.

Those results are quite promising in view of modifying classical electrolyte used in molten carbonate cells such as fuel cell or electrolysis cell. A lot of work is still required because ionic conductivity is not enough to fully qualify a composition as electrolyte. Nevertheless, as carbonates are quite corrosive towards NiO-based electrode and bipolar plates, oxycarbonates could have less impact. Another way would be to make a composite associating these new phases with solid oxide phase such as ceria-based ones in order to increase the conductivity even lowering the operating temperature. This assumption is already under work and the first results are highly promising.

Associated Content

Supporting Information

PXRD pattern of a sample synthesized without lithium, Experimental PXRD pattern of $Na_6Li_4WO_4(CO_3)_4$ showing the presence of Na_2WO_4 as impurity (a) and calculated PXRD pattern from the structural data (b), Observed, calculated and difference PXRD patterns of $Na_6Li_4MoO_4(CO_3)_4$, DSC curves of $Na_6Li_4WO_4(CO_3)_4$ during heating and cooling, PXRD patterns of $Na_6Li_4MoO_4(CO_3)_4$ before and after the melting, Thermal PXRD pattern evolution of $Na_6Li_4MoO_4(CO_3)_4$, Evolution of the cell parameters of $Na_6Li_4MO_4(CO_3)_4$ (M = W, Mo), Nyquist plots of $Na_6Li_4MoO_4(CO_3)_4$ in the solid and molten state, Arrhenius diagrams of $Na_6Li_4WO_4(CO_3)_4$ in the solid and molten state, Anisotropic displacement parameters for $Na_6Li_4WO_4(CO_3)_4$, Structure data of $Na_6Li_4MoO_4(CO_3)_4$, Reliability factors and cell parameters for $Na_6Li_4MO_4(CO_3)_4$ (M = W, Mo). (PDF).

Acknowledgements

The authors thank Denis Mounier (IMMM, Le Mans) for SHG measurements. The X-ray diffractometer and the SEM used in this study belong to instrumental platforms of the "Institut des Molécules et Matériaux du Mans" (IMMM) : "Plateforme de Diffusion et Diffraction des Rayons-X" and "Plateforme de Microscopie Electronique" .

Figures caption

Figure 1: IR spectrum of $Na_6Li_4WO_4(CO_3)_4$.

Figure 2: Observed, calculated and difference PXRD patterns of $Na_6Li_4MoO_4(CO_3)_4$ in the Pm-3m space group by full pattern matching refinement mode. The verticals bars are related to the calculated Bragg reflection positions.

Figure 3: SHG signal for $Na_6Li_4WO_4(CO_3)_4$ and $Na_6Li_4MoO_4(CO_3)_4$.

Figure 4: View of the $Na_6Li_4WO_4(CO_3)_4$ structure showing an isolated WLi_4O_{16} unit, CO_3^{2-} groups and the NaO_8 polyhedra (distorted cube for Na1 and trigonal dodecahedron for Na2)

Figure 5: Partial view of $Na_6Li_4WO_4(CO_3)_4$ structure showing how a CO_3^{2-} group connects three WLi_4O_{16} units together.

Figure 6: DSC curves of $Na_6Li_4MoO_4(CO_3)_4$ oxycarbonate, (a) heating at $2°C.min^{-1}$ in 100% CO_2 and (b) cooling at $2°C.min^{-1}$, in 100% CO_2.

Figure 7: Arrhenius diagram of $Na_6Li_4MoO_4(CO_3)_4$ solid phase for three atmosphere compositions (CO_2 100%, CO_2-air 70-30%, CO_2-air 20-80%) and during one heating/cooling cycle each time.

Figure 8: Arrhenius diagram of the molten $Na_6Li_4MoO_4(CO_3)_4$ phase as a function of the atmosphere composition (CO_2 100%, CO_2-air 70-30%, CO_2-air 20-80%) and during one heating/cooling cycle each time.

References

(1) McPhail, S. J.; Leto, L.; Della Pietra, M.; Cigolotti, V.; Moreno, A. International Status of Molten Carbonate Fuel Cells Technology. ENEA: National Agency for New Technologies, Energy and Sustainable Economic Development. **2015** Available online at: http://www.enea.it/it/pubblicazioni/pdfdossier/2015_MCFCinternationalstatus

(2) Rashidi, R.; Berg, P.; Dincer, I. Performance investigation of a combined MCFC system. *Int. J. Hydrogen Energy* **2009,** 34, 4395-4405.

(3) Spinelli, M.; Di Bona, D.; Gatti, M.; Martelli, E.; Vigano, F.; Consonni, S.; Assessing the potential of molten carbonate fuel cell-based schemes for carbon capture in natural gas-fired combined cycle power plants. *J. Power Sources* **2020**, 448, 227223.

(4) Kojima, T.; Miyazaki, Y.; Nomura, K.; Tanimoto, K. Electrical conductivity of Molten Li_2CO_3-X_2CO_3 (X: Na, K, Rb and Cs) and Na_2CO_3-Z_2CO_3 (Z: K, Rb and Cs). *J. Electrochem. Society* **2007**, 154, F222-F230.

(5) Morita, H.; Kawase, M.; Mugikura, Y.; Asano, K.; Degradation mechanism of molten carbonate fuel cell based on long-term performance: Long-term operation by using bench-scale cell and post-test analysis of the cell. *J. Power Sources* **2010,** 195, 6988-6996.

(6) Huijsmans, J.P.P.; Kraaij, G.J.; Makkus, R.C.; Rietveld, G.; Sitters, E.F.; Reijers, H.Th.J. An analysis of endurance issues for MCFC. *J. Power Sources* **2000**, 86, 117-121.

(7) Patent, US 5942345, Kaun, Thomas D.; Roche, Michael F.

(8) Mihui, L.; Chang-Whan, L.; Hyung-Chul, H.; Jonghee, H.; Sung Pil, Y.; Ki Bong, L. Mechanical strength improvement of aluminum foam-reinforced matrix for molten carbonate fuel cells. *Int. J. Hydrogen Energy* **2017**, 42, 16235-16243.

(9) Soares, C.M.C.; Patrício, S.G.; Figueiredo, F.M.L.; Marques, F.M.B. Relevance of the ceramic content on dual oxide and carbonate-ion transport in composite membranes. *Int. J. Hydrogen Energy* **2014**, 39, 5424-5432.

(10) Bae, J.K.; Kim,H.-W.; Accardo, G.; Kim, G. S.; Ham, H. C.; Jang, S.-C.; Cho, Y. S.; Yoon, S. P. Study on LiI and KI with low melting temperature for electrolyte replenishment in molten carbonate fuel cells. *Int. J. Hydrogen Energy* **2019**, 44, 25930-25938.

(11) Arfaoui, J.; Ghorbel, A. ; Petitto, C.; Delahay, G. New MoO_3-CeO_2-ZrO_2 and WO_3-CeO_2-ZrO_2 nanostructured mesoporous aerogel catalysts for the NH_3-SCR of NO from diesel engine exhaust. *J. Ind. Eng. Chem.* **2021**, 95, 182-189.

(12) Ramana, C.V.; Mauger, A.; Julien, C.M. Growth, characterization and performance of bulk and nanoengineered molybdenum oxides for electrochemical energy storage and conversion. *Prog. Cryst. Growth and Charact. Mater*. **2021**, 67, 100533.

(13) Georges, S.; Goutenoire, F.; Bohnke, O.; Steil, M. C.; Skinner, S. J.; Wiemhoefer, H.-D.; Lacorre, P. The LAMOX Family of Fast Oxide-Ion Conductors: Overview and Recent Results. *J. New. Mat. Electrochem. Systems* **2004**, 7, 51-57.

(14) Lacorre, P.; Goutenoire, F.; Bohnke, O.; Retoux, R.; Laligant, Y. Designing fast oxide-ion conductors based on $La_2Mo_2O_9$. *Nature 2000*, 404, 856–858.

(15) Srijith, L.; Das, A.; Dasari, H. D.; Saidutta, M. B. Electrical conductivity studies on LAMOX based electrolyte materials for solid oxide fuel cells. *Ceram. Int.* **2022**, 48, 29229-29237.

(16) Rodriguez-Carvajal, J. Program FULLPROF Version September 2020, Institut Laue-Langevin, Grenoble.

(17) Sheldrick, G. M. SHELXS97, Program for Crystal Structure Solution and Refinement, University of Göttigen, Germany, 1997

(18) Dougherty, J.P.; Kurtz, S. K. A second harmonic analyser for the detection of non-centrosymmetry. *J. Appli. Crystallogr*. **1976**, 9, 145-158

(19) Lair, V.; Albin, V.; Ringuede, A.; Cassir, A. Theoretical predictions vs. experimental measurements of the electrical conductivity of molten Li_2CO_3-K_2CO_3 modified by additives.

Int. J. Hydrogen Energy, **2012**, 37, 19357-19364.

(20) Imanaka, N.; Masui, T.; Mayama, Y.; Koyabu, K. Synthesis of crystalline yttrium oxycarbonate in a single phase. *J. Solid State Chem.* **2005**, 178, 3601–3603

(21) Shannon, R. D. Revised Effective Ionic Radii and Systematic Studies of Interatomie Distances in Halides and Chaleogenides. *Acta Cryst*. **1976**, A32, 751-767

(22) Jiang, Y.; Sun, Y.; Bruno, F.; Li, S. Thermal stability of Na_2CO_3-Li_2CO_3 as a high temperature phase change material for thermal energy storage. *Thermochim. Acta*. **2017**, 650, 88-94.

(23) Steele, B.C.H. Material science and engineering: The enabling technology for the commercialisation of fuel cell systems. *J. Mater. Sci*. **2001**, 36, 1053–1068.